J Mater Sci (2010) 45:1100–1106
DOI 10.1007/s10853-009-4052-0

Preparation and characterization of magnetic carbon nanomaterials bearing APTS–silica on their surface

Urszula Narkiewicz · Iwona Pełech · Marcin Podsiadły · Michał Cegłowski · Grzegorz Schroeder · Joanna Kurczewska

Received: 30 May 2009 / Accepted: 18 November 2009 / Published online: 1 December 2009

Abstract The formation of metal-encapsulated carbon nanomaterials by using metallic catalysts (iron, cobalt, and nickel) has been studied. Moreover, these materials were coated with silica surface modified by (3-Aminopropyl)-trimethoxysilane (APTS). Each intermediate structure was confirmed by X-ray diffraction (XRD) and transmission electron microscopy (TEM). The surface morphology of silica-coated carbon nanomaterials was analyzed by scanning electron microscopy (SEM). The modified, APTS–silica surface was additionally characterized by Fourier transform infrared spectroscopy (FT-IR), elemental (EA), and thermogravimetric analysis (TGA).

Introduction

Carbon nanomaterials, both carbon nanotubes (CNTs) and nanocapsules, can be synthesized using different methods: arc discharge, laser ablation, and catalytic chemical vapor deposition (CCVD). The latter generally involves decomposition of carbon-containing molecules such as carbon oxide or hydrocarbons, usually methane, acetylene or ethylene [1–6], on the metal particles. Best results are obtained with iron, nickel, and cobalt nanoparticles as catalyst. The CCVD method is carried out under mild preparation conditions, the production costs are low, is also easy to control the process, and to up-grade its scale.

Magnetic carbon nanomaterials have many applications, including magnetic data storage, magnetic toners in xerography, magnetic inks, or ferrofluids [7, 8]. Additionally, nanotubes filled with metals may provide elements for nanoscale electrical or electronic devices such as amplifiers, switches, or electrical–mechanical converters [9]. However, nanocrystalline metals are very sensitive to environmental degradation, because of their high ratio of surface area to volume and high reactivity. The coating of metal nanocrystals with graphitic layers may protect them against environmental degradation. The coating can also endow these particles with biocompatibility and make the carbon-encapsulate particles useful in bio-engineering applications [10, 11].

CNTs coated with inorganics are recently of great interest because of combined properties of different materials. Silica-coated carbon nanotubes are widely practiced as they find variety of applications [12]. There are several methods of preparation of such nanomaterials. CNTs are firstly functionalized covalently or noncovalently and then participate in the synthesis of silica on their surface. On the other hand, silica particles could be beforehand modified and then react with carbon nanotubes surface [13]. Nevertheless, the initial synthetic step requires modification of CNTs surface through chemical oxidation at high temperature [14] or chemical oxidation in the presence of phase transfer catalysts [15]. Kim et al. activated silica nanotubes by vinyl [16] or amine [17] groups from silane coupling agents. Liu [18] prepared CNTs encapsulated by polyacrylaminopropylsiloxane. Apart from methods discussed, it is also possible to cover CNTs with inorganic silica in a sol–gel process, which precludes the structure destruction of CNTs [19]. Moreover, it could be interesting to combine

U. Narkiewicz · I. Pełech · M. Podsiadły
Institute of Chemical and Environment Engineering, West Pomeranian University of Technology, Pułaskiego 10, 70-322 Szczecin, Poland

M. Cegłowski · G. Schroeder · J. Kurczewska (✉)
Faculty of Chemistry, Adam Mickiewicz University, Grunwaldzka 6, 60-780 Poznan, Poland
e-mail: asiaw@amu.edu.pl

properties of both magnetic carbon nanomaterials and silica particles. Deng [20] synthesized magnetic silica nanoparticles functionalized CNTs.

This paper presents the synthesis and characterization of functionalized carbon nanomaterials (carbon nanotubes and nanocapsules). The initially synthesized materials containing metals (Fe, Co, Ni) are coated with silica in a sol–gel process. Finally, the silica surface is modified with silane coupling agent having amine groups—(3-Aminopropyl)-trimethoxysilane (APTS).

Experimental

Synthesis of magnetic carbon nanomaterials

Nanocrystalline iron was obtained by a fusion of magnetite (Fe_3O_4) with a small amount of promoter oxides (Al_2O_3, CaO) in an electric furnace. The obtained alloy was crushed and sieved in order to obtain a fraction of 1.2–1.5 mm. This alloy was reduced under hydrogen. As a result of reduction, nanocrystalline iron was obtained and the promoters remained in the oxide state. In order to avoid rapid oxidation, the samples were passivated under nitrogen containing traces of oxygen.

Nanocrystalline cobalt and nickel were obtained from cobalt (II) nitrate and nickel (II) nitrate by addition of a small amount of calcium and aluminum nitrates. The salts were dissolved in water and 20% NH_4OH was added as a precipitating agent, to obtain pH of 8. The metal hydroxides were precipitated from the solution and the deposit was washed with water, filtered and dried at 75 °C. The next step was calcinations at 500 °C for 1 h to obtain the precursor of nanocrystalline cobalt–cobalt oxide and nanocrystalline nickel–nickel oxide (with small amount of structural promoters—CaO and Al_2O_3). The powder samples of cobalt oxide and nickel oxide obtained were pressed, crushed, and sieved to obtain the grain size fraction in the range of 1.2–1.5 mm.

All catalysts, before ethylene decomposition, were reduced polythermally at the temperatures rising from 20 to 500 °C. After this treatment, the hydrogen flow was replaced by ethylene. The synthesis was performed under atmospheric pressure at 500 °C (nickel catalyst) or 700 °C (iron and cobalt catalyst) and lasted 60 (nickel and cobalt catalyst) and 180 min (iron catalyst). After ethylene decomposition, the samples were cooled to room temperature under argon flow. The values of relative mass change for all samples are presented in the Table 1.

Synthesis of magnetic carbon nanomaterials bearing APTS-silica

Magnetic carbon nanomaterials bearing APTS–silica were prepared following the procedure outlined in Scheme 1.

Metal-encapsulated silica-coated carbon nanomaterials (sol–gel technique)

Sodium silicate water solution (27% SiO_2 in 14% NaOH; 7 mL) and metal-encapsulated (iron, cobalt) carbon nanotubes or (nickel) nanocapsules (0.35–0.45 g) were introduced into the beaker equipped with a mechanical stirrer. The mixture was then diluted by distilled water (to 150 mL) and mechanically stirred in the ultrasonic bath for 30 min at room temperature. After that the temperature was increased up to 80 °C and hydrochloric acid was added to adjust the pH to 6–7 value. The iron-, cobalt- or nickel-encapsulated silica-coated carbon nanomaterials obtained were filtered using glass microfiber filter and washed repeatedly with distilled water and methanol.

Table 1 Experimental conditions of metal–carbon composites obtaining and values of relative mass change for these materials

Catalyst	Experimental conditions			The relative change of mass (gC/gMe) where Me–Fe, Ni, or Co
	Gas or gases mixture	Temperature (°C)	Time (min)	
Iron	Ethylene–argon	700	180	5.1
Nickel	Ethylene	500	60	6.5
Cobalt	Ethylene	700	60	1.5

Scheme 1 Synthesis of magnetic carbon nanomaterials bearing APTS–silica

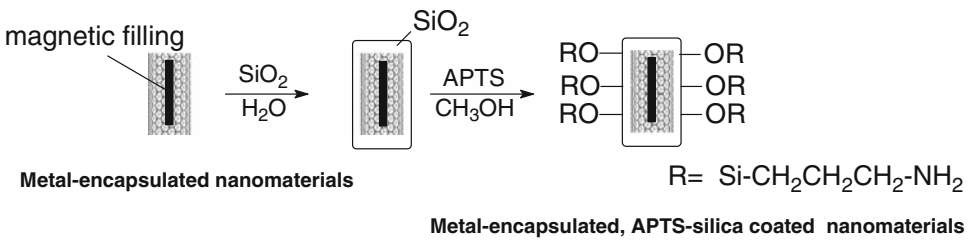

Silanization procedure

Metal-encapsulated silica-coated carbon nanomaterials were suspended in methanol (25 mL), then distilled water (1 mL) and glycerol (25 mL) were added. The suspended solids were mechanically stirred in the ultrasonic bath for 30 min at room temperature. Then they were introduced into a three-necked round bottom flask equipped with a mechanical stirrer and a reflux condenser. (3-Aminopropyl)-trimethoxysilane (Aldrich) (0.1 g) was added dropwise to the reaction mixture and heated (90 °C) for 3 h. The final products, iron (**1**)-, cobalt (**2**)-, or nickel (**3**)-encapsulated carbon nanomaterials bearing APTS–silica were filtered and washed repeatedly with distilled water and methanol. Finally, they were dried under vacuum at room temperature.

Elemental analysis found: **1** N, 3.30; C, 14.75; H, 3.61; **2** N, 1.91; C, 10.97; H, 1.88; **3** N, 2.08; C, 13.55; H, 2.07.

Chemicals and apparatus

The phase composition of the catalysts and the samples after ethylene decomposition was characterized using X-ray diffraction method (Philips X'Pert). The mean crystallite size of the catalyst was determined using X-ray diffraction method and calculated using the Scherrer's equation. X-ray diffraction of silica-coated nanomaterials was measured using Brucker D8 Advance powder diffractometer equipped with Johansson monochromator (λCu $K_{\alpha 1}$ = 1,5406 Å) and silicon strip detector LynxEye.

The chemical composition of the catalyst samples was determined using ICP–AES (Inductively Coupled Plasma Atomic Emission Spectroscopy) method (JY 238 Ultrace equipment from Jobin–Yvon). The role of promoter oxides was to stabilize the nanocrystalline iron structure at elevated temperatures.

The IR spectra were recorded on IFS 66v/s FT-IR spectrophotometer from Bruker, equipped with a MCT detector (128 scans, resolution 2 cm^{-1}).

Surface morphology of silica-coated nanomaterials was studied by a Carl Zeiss EVO-40 scanning electron microscope, SEM (resolution 3 nm, magnification ×1000000). Transmission electron microscope (TEM) studies were performed by JEM-1200 EXII microscope to monitor the morphology and structural properties of all samples. The materials for TEM were sonicated in acetone and then one droplet was put onto a copper grid coated with holey carbon grid.

Elemental analysis of the compounds studied was carried out on a Vario ELIII (Elementar, USA) analyzer, while thermogravimetric studies—in a Setaram TGA at a heating rate of 10 °C/min under helium atmosphere.

Copper perchlorate was commercial product of Aldrich and was used without any purification. Doubly distilled water was used for the solution preparation (0.5 mol dm^{-3}).

Results and discussion

The mean crystallite size of the catalysts and the content of promoter oxides are presented in Table 2. The phase composition of iron, cobalt and nickel catalysts is shown in Fig. 1. According to XRD analysis, the sample of iron catalyst contains two phases: iron and iron oxide (Fig. 1, spectrum 1). Small iron crystallites are very sensitive to oxidation and in contact with air the sample is partially oxidized. The same effect is observed for the sample of cobalt catalyst (Fig. 1, spectrum 2). Additionally, in this sample two crystallography phases are present: hexagonal closed-packed (hcp-Co) and face-centered cubic (fcc-Co). For pure cobalt the former structure is stable at room temperature. The latter structure exists above 422 °C and is not stable at room temperature [21]. Addition of structural promoters probably leads to stabilization of this fcc-Co form. In the sample of nickel catalyst (Fig. 1, spectrum 3), only one phase of metallic nickel is present. The peaks originating from nickel oxide are not observed. We cannot exclude the formation of a passive layer of nickel oxide but the sensitivity of X-ray diffraction method is not sufficient to detect a small amount of this phase.

Table 2 Percentage of promoter oxides in the catalyst and the mean crystallite size

Catalyst	CaO (%)	Al_2O_3 (%)	Mean crystallite size (nm)
Iron	3.0	2.9	17
Nickel	0.8	3.6	25
Cobalt	0.2	1.5	90

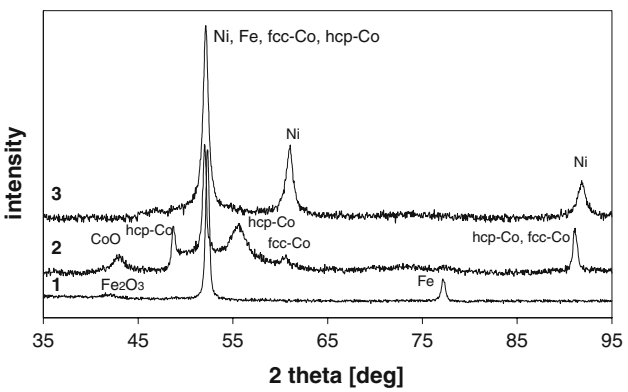

Fig. 1 Diffraction patterns of iron (1), cobalt (2), and nickel (3) catalysts before ethylene decomposition

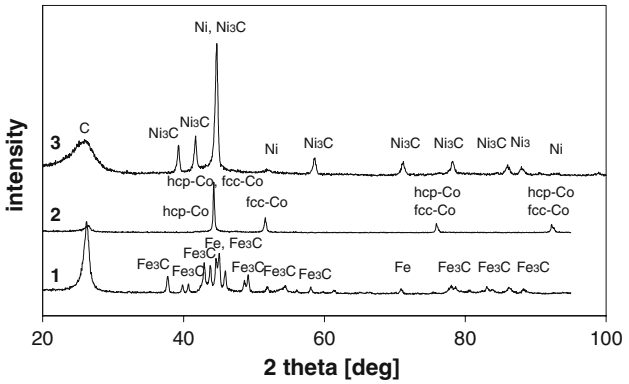

Fig. 2 Diffraction patterns of iron (1), cobalt (2), and nickel (3) catalysts after ethylene decomposition

The diffraction patterns of iron, cobalt, and nickel catalyst after ethylene decomposition are presented in Fig. 2. The diffraction pattern of the iron sample (Fig. 2, spectrum 1) shows peaks characteristic of cementite. In the experimental conditions, other iron carbides are not observed. Unconverted iron is also present which indicates that not all iron was converted to cementite. In this case, the peak assigned to graphite at $2\Theta = 26°$ is observed like as in the XRD pattern of the cobalt sample (Fig. 2, spectrum 2). Carbon coats the metal particles and protects the surface against oxidation in air. So the peaks attributed to cobalt oxide are not found in the XRD pattern of this sample. On the diffraction pattern peaks derived from both hcp-Co and fcc-Co phases are visible, however, the intensity of the former phase is lower than of the latter. We conclude that the higher carbon content in the sample better stabilize high temperature cobalt structure in the room temperature. The diffraction pattern of the nickel catalyst (Fig. 2, spectrum 3) shows the peaks corresponding to nickel carbide and graphite. A small amount of unconverted nickel is also present.

The morphology of carbon deposits after ethylene decomposition was also investigated. The images of the deposit synthesized on the iron (Fig. 3a, b) sample reveal numerous multiwalled carbon nanotubes. The diameters of these structures are of the order of 10–40 nm. TEM observation also reveals some defects formed during the growth of the tubes, leading to changes in the growth direction. We can also observe the formation of amorphous carbon on the outer surface of carbon nanotubes. A part of metal particles was found inside the tubes.

In the case of cobalt catalyst (Fig. 3c, d) carbon nanotubes and catalyst particles encapsulated in carbon were simultaneously obtained. At the end of CNTs some cobalt crystallites were visible. This indicates that the main growth mode followed a tip growth mechanism [22]. The diameters of these structures were in the range from 10 to 30 nm. The graphene layers were not parallely orientated

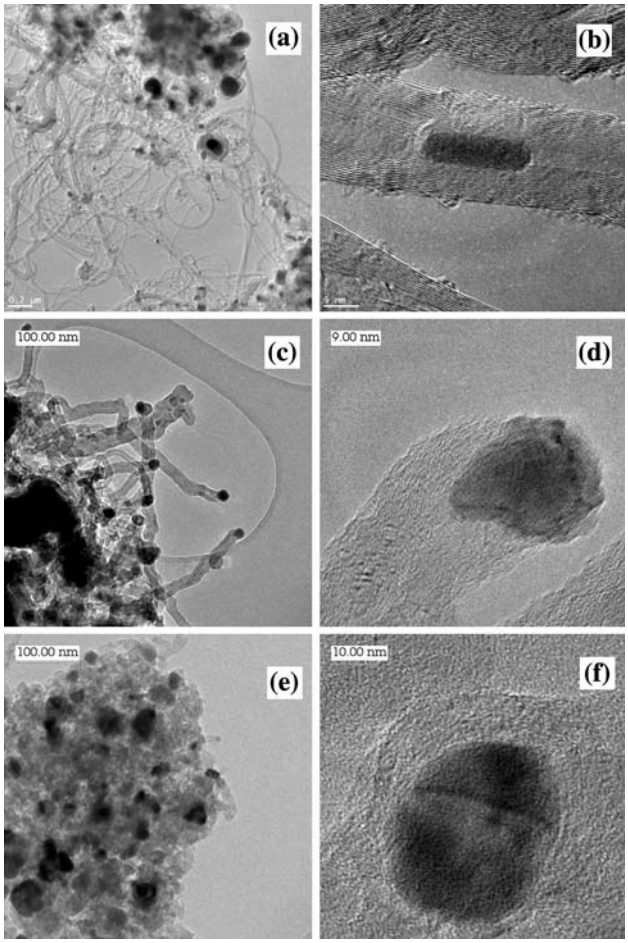

Fig. 3 TEM images of iron (**a**, **b**), cobalt (**c**, **d**), and nickel (**e**, **f**) catalysts after ethylene decomposition at 700 °C (iron, cobalt) and 500 °C (nickel)

in respect to the fiber axis and the angle between the fiber axis and the graphene plane was of 35–45°. When the catalyst particles were larger than 100 nm, carbon-coated catalyst particles were obtained. TEM image of these nanoparticles shows a metallic core and a graphitic shell. The interplanar distance between two adjacent graphene planes is about 0.340 nm, close to the (002) lattice distance in graphite (0.335). The observed higher lattice spacing is attributed to the defects in the graphite structure. The thickness of the coating was around 20 nm.

The main product of ethylene decomposition on the nickel catalyst was composed of the catalyst particles encapsulated in carbon (Fig. 3e, f). The carbon coating has a crystalline graphite structure. The interplanar distance between two adjacent graphene planes is about 0.340 nm. The thickness of the coating is around 10 nm.

Figure 4 presents the XRD patterns of metal-encapsulated, silica-coated carbon nanomaterials. No crystalline SiO_2 phase is found because silica forms amorphous coating on carbon nanomaterials surface. The broad halo at

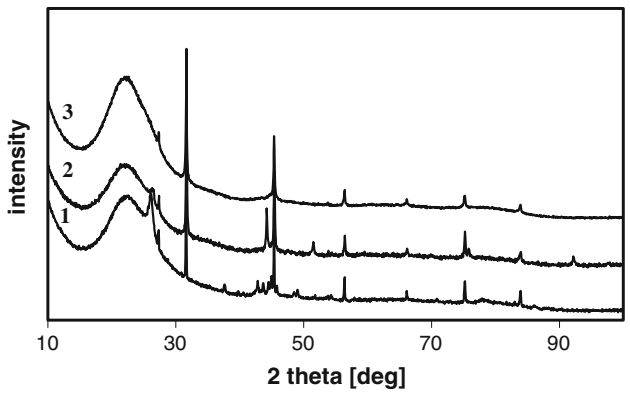

Fig. 4 Diffraction patterns of iron (1), cobalt (2), and nickel (3)-encapsulated, silica-coated carbon nanomaterials

$2\Theta = 22°$ and low intensity of silica diffraction peaks confirms amorphous state of SiO_2. On the other hand, the diffraction peak at $2\Theta = 26°$ corresponding to carbon (graphite) is present, which indicates that silica coating is not destructive for crystal structure of carbon nanomaterials.

The TEM images of metal-encapsulated, silica-coated carbon nanomaterials and magnetic carbon nanomaterials bearing APTS–silica are shown in Fig. 5. In general, silica and APTS–silica cover make a uniform layer but a few coarse and sidewalls are also present.

Scanning electron microscopy (SEM) was used to examine the morphology of silica and APTS–silica-coated carbon nanomaterials. Fig. 6 presents SEM micrographs in different magnifications. The samples consisted of particles with the size ranging from 20 to 40 μm, but some larger ones were also observed. All particles were characterized by no peculiar shape. No aggregates were present in the sample. Nevertheless, SEM images evidence the presence of unmodified and modified silica on the carbon nanomaterials surface.

The formation of organic, APTS pendant arms on silica-coated carbon nanomaterials was additionally confirmed by IR spectroscopy, elemental, and thermogravimetric analysis. The IR absorption peaks of Si–O–Si bands appear at 1084, 780, and 462 cm^{-1} after silica-coated treatment (Fig. 7). A band appearing at 3400 cm^{-1} is assigned to the N–H and O–H stretching vibrations region, while the peak appearing at 2915 cm^{-1} corresponds to the C–H stretching of alkyl groups. The presence of IR peaks assigned to O–H groups (3400 and 1615 cm^{-1}), could be caused by water molecules adsorption on the carbon surface in the sol–gel

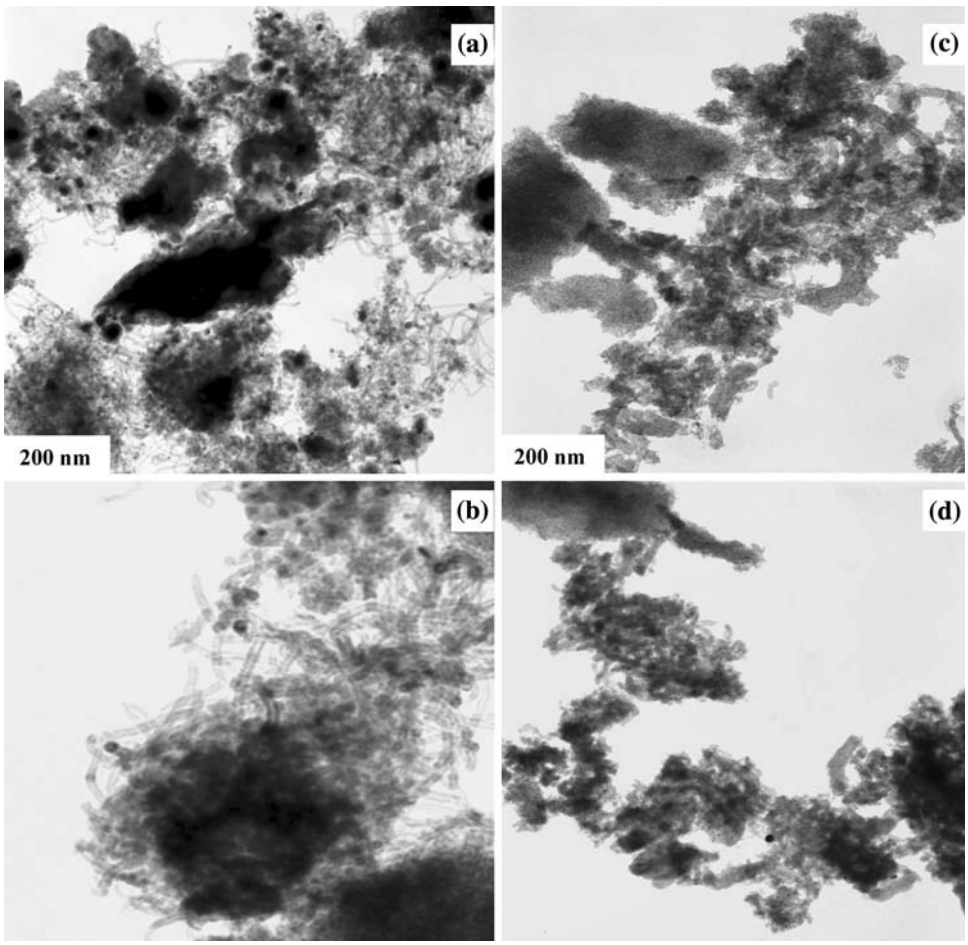

Fig. 5 TEM images of cobalt (**a**)- or nickel (**c**)-encapsulated, silica-coated carbon nanomaterials and cobalt (**b**)- or nickel (**d**)-encapsulated carbon nanomaterials bearing APTS–silica

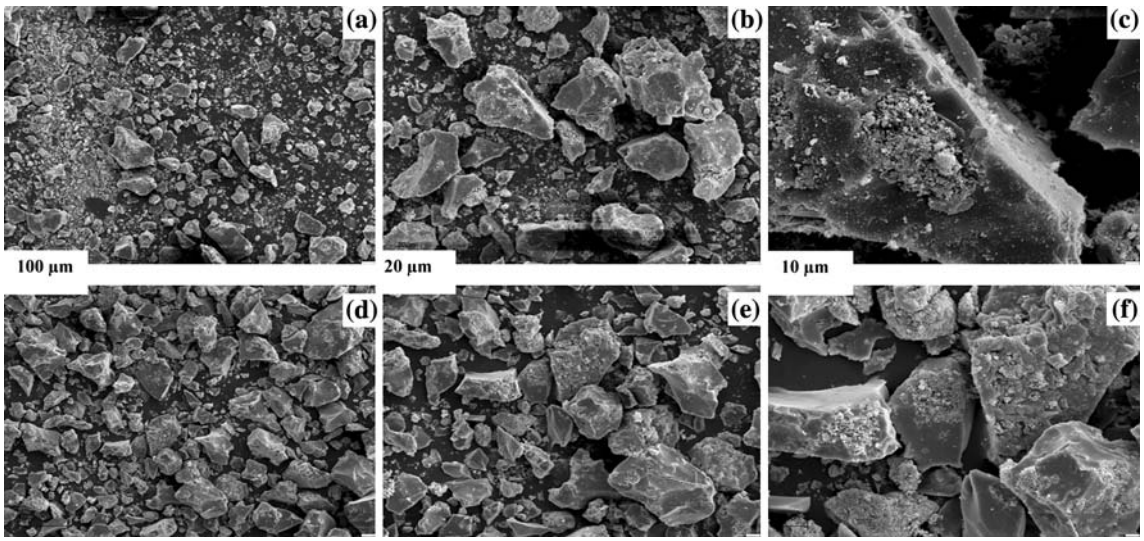

Fig. 6 Scanning electron micrographs of iron-encapsulated, silica-coated carbon nanomaterials (**a**, **b**, **c**) and iron-encapsulated carbon nanomaterials bearing APTS–silica (**d**, **e**, **f**)

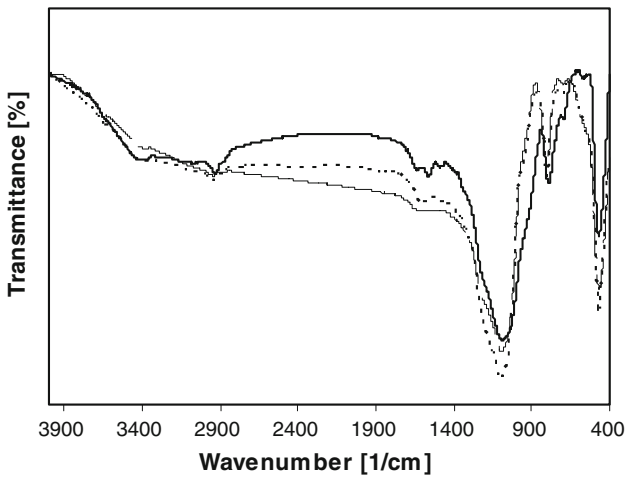

Fig. 7 FT-IR spectra of Fe (——), Co (— — —), Ni (- - - - - -) encapsulated, silica-coated carbon nanomaterials

process. According to the elemental analysis data, the percentage of the surface modification by APTS–silica is rather comparable. However, some differences are observed and the modification percentage can be ordered as follows: Fe > Ni > Co-encapsulated, APTS–silica-coated carbon nanomaterials. The weight content of organic groups was also analyzed by TG analysis. Thermogravimetric curves show loss of mass as an effect of continuous heating in helium atmosphere. The first insignificant mass loss is caused by physically adsorbed solvent applied in the synthesis. Further mass loss is observed until 950 K (mass loss of about 20%) due to elimination of a part of the ligand (organic groups) and some silanol groups. After that, a constant weight is observed, which is probably caused by the remaining of silica on carbon nanomaterials surface.

The supports studied demonstrate magnetic properties (Fig. 8a) and could be applied in the scavenging of various

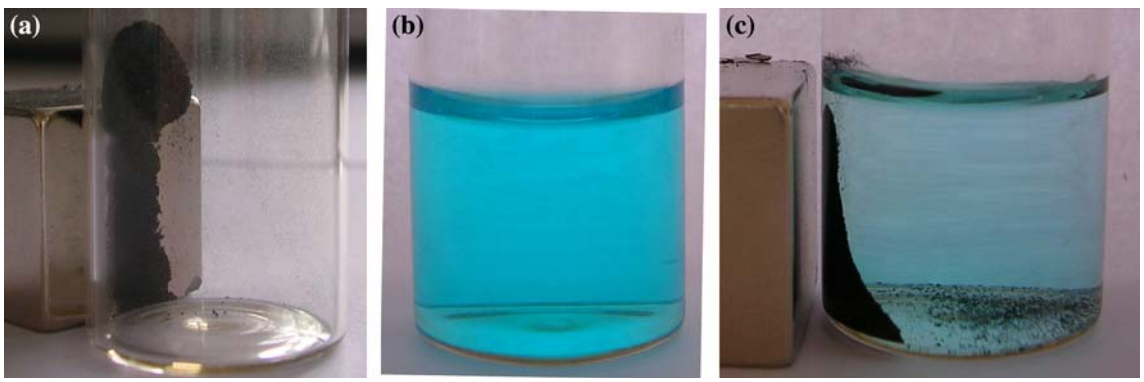

Fig. 8 Removal of copper(II) cations from the solution by magnetic metal-encapsulated, silica-coated carbon nanomaterials

ions from aqueous solutions. Figures 8b–c demonstrates the scavenging ability of copper ions from the solution by the metal-encapsulated, silica-coated carbon nanomaterials. The copper solution experienced the color intensity decrease in the presence of the support studied as an effect of Cu(II) complexing by the solid surface. Moreover, the incorporation of magnet causes the scavenger concentration in the magnetic field. Therefore, magnetic properties of the supports discussed facilitate removal of complexed ions from the solutions.

Conclusions

In conclusion, successful synthesis of metal-encapsulated, APTS–silica-coated carbon nanomaterials was demonstrated. The application of sol–gel process to prepare silica assemblies on carbon nanomaterials allowed the formation of magnetic silica carbon nanomaterials activated by amine groups in high yield. Moreover, the combination of magnetic properties of carbon nanomaterials and activated silica surface offers potential application for the development of biosensors. The presence of nitrogen donor atoms in functionalized silica surface suggests the application of such stable structures as selective extraction tools for purification of wastewater.

Acknowledgements The authors are grateful to Dr. E. Borowiak-Paleń (Institute of Chemical and Environmental Engineering, West Pomeranian University of Technology, Szczecin) for the HRTEM images of iron sample after ethylene decomposition.

References

1. Escobar M, Moreno MS, Candal RJ, Marchi MC, Caso A, Polosecki PI, Rubiolo GH, Goyanes S (2007) Appl Surf Sci 254:251
2. Noda KL, Goncalves NS, Valentini A, Probst LFD, De Almeida RM (2007) J Mater Sci 42:914. doi:10.1007/s10853-006-0009-8
3. Singh BK, Ryu H, Chikate RC, Hoa ND, Park SJ, Kim S, Lee JR (2006) Solid State Commun 139:102
4. Tripol'skii AI, Lemesh NV, Strizhak PE (2008) Theor Exp Chem 44:240
5. Khavrus VO, Lemesh NV, Gordijchuk SV, Tripolsky AI, Ivashchenko TS, Biliy MM, Strizhak PE (2008) Kinet Catal Lett 93:295
6. Chai SP, Zein SHS, Mohamed AR (2006) Chem Phys Lett 426:345
7. Liu BH, Ding J, Zhong ZY, Dong ZL, White T, Lin JY (2002) Chem Phys Lett 358:96
8. Kumar B, Tan HS, Ramalingam N, Mhaisalkar SG (2009) Carbon 47:321
9. Zhbanov AI, Sinitsyn NI, Torgashov GV (2004) Radiophys Quantum Electron 47:435
10. Balasubramanian K, Burghard M (2006) Anal Bioanal Chem 385:452
11. Pauser S, Reszka R, Wagner S, Wolf KJ, Buhr HJ, Berger G (1997) Anti-Cancer Drug Des 12:125
12. Liu Y, Tang J, Chen X, Wang R, Pang GKH, Zhang Y, Xin JH (2006) Carbon 44:165
13. Bottini M, Magrini A, Dawson MI, Bergamaschi A, Mustelin T (2006) Carbon 44:1301
14. Satishkumar BC, Govindaraj A, Mofokeng J, Subbanna GN, Rao CNR (1996) J Phys B At Mol Opt Phys 29:4925
15. Zhang N, Xie J, Varadan VK (2002) Smart Mater Struct 11:962
16. Hong S, Kim M, Hong J, Hong CK, Jung D, Shim SE (2008) Synth Met 158:900
17. Kim M, Hong J, Lee J, Hong CK, Shim SE (2008) J Colloid Interface Sci 322:321
18. Liu Y, Zhang C, Du Z, Li C, Li Y, Li H, Yang X (2008) Carbon 46:1670
19. Zhou Z, Wang S, Lu L, Zhang Y, Zhang Y (2008) Compos Sci Technnol 68:1727
20. Deng Y, Deng C, Yang D, Wang C, Fu S, Zhang X (2005) Chem Commun 44:5548
21. Ullmann's encyclopedia of industrial chemistry (2004) 6th edn, CD-ROM version
22. Sinnott SB, Andrews R, Qian D, Rao AM, Mao Z, Dickey EC, Derbyshire F (1999) Chem Phys Lett 315:25